High Frequency Oscillations in Epilepsy
OTKA-PD101754
Daniel Fabo

Final report

Background

Short high frequency oscillation (HFO, higher than 80Hz) packages called ripples gained increasing significance in the last decade in the field of focal epilepsy. HFOs were described in the hippocampal region of the rat (Buzsáki et al. 1992), but was demonstrated in the temporal lobe of human epileptic patients (Bragin et al. 1999). During physiological sleep and relaxation sharp wave-ripple complexes contribute to the memory consolidation process of hippocampal dependent memory traces (Sirota et al. 2003; Ramadan et al. 2009). In pathological conditions these oscillations participate in various kinds of focal epilepsy related brain activities like interictal discharge (IID) genesis (Urrestarazu et al. 2007), seizure genesis (Bragin et al. 2004) and epileptogenesis (Jacobs et al. 2009). Ripples were shown to localize into the seizure focus in humans (Jacobs et al. 2008), near the epileptogenic lesion (Staba et al. 2007), and the removal of the ripple generating area was a good predictor of seizure freedom after epilepsy surgery (Jacobs et al. 2010). Based on these ground breaking observations it seems that ripple oscillations are key players in the epileptogenic process, and the removal of them makes the brain impossible to generate epileptic seizures. On the other hand it is possible that these oscillations have some role in physiological processes, but the characterization of the difference between pathologic and physiologic ripples is missing.

Increasing amount of data is available on the neurobiological processes during sleep and the intracortical generators of slow wave activity (Cash et al. 2009; Csercsa et al. 2010). Two functional states in the cortex alternate continuously during the slow-wave activity. These are the up-states, which are accompanied by upper layer sink and middle layer source in the neocortex and large amount of high frequency (in the beta, gamma range) activities, and the down-states that are characterized by middle layer sinks and upper layer sources and non specific de-activation of the cortex with the absence of higher frequency activities (Amzica and Steriade 1995). Recent data show that ripple activities are grouped by this slow oscillation and show up only in the up-state, and is fine tuned to the spindle oscillations (Clemens et al. 2007; 2011). Spindle oscillations are known for their role in memory consolidation processes (Clemens et al. 2005; 2006). It has been shown, that ripple oscillations coincide with IID in a high proportion (60-70%) in humans (Urrestarazu et al. 2007). These data allow us to hypothesize a strong link between slow oscillations, IIDs, and ripple oscillations in the cortex, the strength of which link hasn't been evaluated though.

Two types of ripple oscillations were demonstrated both in the rodent hippocampus (Bragin et al. 2004)and in human temporal lobe (Staba et al. 2002). The central frequency of the slower type ripple was around 100Hz, while it was around 250Hz for the faster type. We will call them slow ripples and fast ripples respectively to avoid terminological confusions. The relative abundance of the fast ripples lateralized to the seizure-prone side in human temporal lobe epilepsy, while the opposite was true for the non-seizure originating side, there the slow ripples outnumbered the fast ones (Staba et al. 2004). Based on this observation the authors concluded that slow ripples participate in physiological processes and the fast ripples are pathologic activities (Engel et al. 2009). There is no data on the relationship of these oscillations however and we don't know how much do they coincide with eachother. There were no attempts to record ripple oscillations in the human cortex in order to describe their intracortical generators, thus we don't know that fast ripples are similar to slow ripple or they have completely different cortical generators.

The effect of cortical electrical stimulation (CES) was studied in epilepsy. The presence of long latency (>100 ms) evoked IIDs were good markers of epileptogenic area (Valentín et al. 2005). It is not known that these long latency IIDs contain or not ripple oscillations. It is also unknown that do the CES evoke ripple oscillation at any latencies and what is the relationship of the evoked ripples to the epileptogenic zone.

Methods – intrahippocampal recording

Surgery and recording

The intrahippocampal recordings were performed before anterior temporal lobectomy, after video-EEG monitoring procedure of medically intractable mTLE patients with unilateral seizure starting. The seizure onset zone identifying procedure and electrode implantations and surgeries were done in the Epilepsy Centre of the National Psychiatry and Neurological Institution (2004-2007) and National Institute of Clinical Neurosciences (NICN).

Fourteen patients were included in the acute hippocampal recording study, all of them was consented and informed of the risks. The permission to the experimental process was given from the Hungarian Medical Research Council, in accordance with the Declaration of Helsinki. During the epilepsy surgery, before the temporal lobe resection with a special kind of experimental setup, we tried to elicit evoked potentials from the human hippocampus. The technique was previously described in Fabo 2007(Ulbert et al. 2001; Fabó et al. 2008). Briefly, we used a microelectrodes to record in vivo activity from the hippocampus and an eight contact strip electrode placed around the temporal pole (Ad-Tech Medical Instrument Corporation, Racine, USA) to stimulate the temporal input pathways of the hippocampus. The tip of the multielectrode was positioned to the surface of the hippocampus through a small cut of the lateral ventricle and slowly slipped into the brain tissue with 2-4 mm increments. The microelectrode insertion was done by a precision hydraulic micro-manipulator with approximately 200 µm/sec speed, which minimalized the traumatic effect. The micro-manipulator structure gave the opportunity to hold one or two microelectrodes, so in some cases, two parallel electrodes were inserted with 6 mm distance. The field potential gradient recording was continuous during the insertion and the extraction. The used multielectrode (ME) was described previously (Heit et al. 1999; Ulbert et al. 2001; 2004), originally developed to record the electrical activity from the layers of the neocortex. This was not applicable for hippocampal recording, so our research group designed a deep multielectrode (dME) to record from the internal brain structures. The 24 contacted dME (linearly arranged contacts, Ø: 25µm, Platinum-Iridium wires, 100 µm or 200 µm center to center distance, first contact is 5 mm far from the tip) is a 10 centimeters long, 350 µm diameter, stainless steel needle. The recordings was taken with custom made equipment, described previously (Ulbert et al. 2001; Fabó et al. 2008). The signal was recorded simultaneously with filtered between 0.1-500 Hz, sampled at 2kHz/channel with 16 bit precision; and filtered between 150Hz-5000Hz, 20kHz/channel on 12 bit.

Low frequency (0.5 Hz, 5-10-15 mA, 0.2 ms pulse duration, 25 or 50 stimuli) stimulation was applied through the adjacent strip electrode contact sites to elicit evoked potentials from the hippocampus. The stimulated electrode distance were calculated from the pole of the temporal lobe and it was agreed to sign the distance in the lateral direction from the pole as negative and positive in the direction of the medial, inner part of the temporal lobe. Ten different stimulation arrangements were -2 - -3 cm, -2 - -1 cm, 0 - -1 cm, where the negative sign illustrates the direction on the outer side of the temporal lobe and 0-1 cm, 1-2 cm, 2-3 cm, 3-4 cm, 4-5 cm, 5-6 cm, 6-7 cm where the stimulations were on the inner side of the temporal pole.

Histology

After the stimulations, the Hippocampal Formation and the Entorhinal Cortex was removed “en-bloc” for histological processing. The histology verified the electrode penetration, and the affected hippocampal structures. This work was done by Zsófia Maglóczky and Lucia Wittner (Ulbert et al. 2004). The penetration of the electrode were identified by light microscopic examination, was reconstructed from multiple stained sections and analyzed in digital picture editing software {Fabo, 2007 #188}. Left panel of Figure 2 shows the reconstructed trajectory and the histology of the electrode penetrations of Pt22.

Data analysis

Local field potential was analyzed in the Edit module of Neuroscan (Neuroscan Inc.) and in Matlab (Mathworks Inc.). We used free accessible, open source Matlab packages, like EEGLAB and Fieldtrip (Donders Institute for Brain, Cognition and Behaviour and the Max Planck Institute in Nijmegen) and previously described {Fabo, 2007 #188} script package developed by our laboratory and self-written Matlab scripts.

To avoid the probable side effect of the stimulation artefact, we replaced it with spline interpolation -4 ms to 4 ms around the artefact transient signal.

Amplitude of evoked potentials

Figure 1 explains the steps of the analysis regarding to the hippocampal layers. Around every stimulation (25-50 pieces occasionally) in a -500 +500 ms window, the hippocampal local field potential data was filtered between 40-500Hz (2nd-order Butterworth) for evoked high frequency activity (EHFA) and between 500-5000Hz (3rd order Butterworth) for multiple unit activity (MUA) from the 20 kHz sampled recordings then Root Mean Square (RMS) calculation was applied in an 11 ms window, 5 times (Figure 2 /C lower box). From the RMS data, the maximal amplitude between +10 to +100 ms after stimulation is measured and converted to statistical z-score value using the mean and standard deviation of the baseline (-450 ms to -50 ms before the stimulation). The z-score amplitude values for EHFO after every stimulation on every channels are color coded and plotted on **Error! Reference source not found.**/D, and the distribution of the Z-score values for EHFA (black) and MUA (light blue) are plotted in the boxplots on **Error! Reference source not found.**/E. The mean amplitude of the multiunit activity across channels were correlated to the mean amplitude of the evoked high frequency activity for all stimulation sessions.

Evoked high frequency activity (EHFA)

We hypothesized that the stimulations evoked putative ripple events therefore we applied 5 z-score threshold on the filtered (40-500Hz) and Root Mean Squared data, similar to the method described by Staba (Staba et al. 2002) to determine the significant evoked high frequency activity.

Evoked ripple (evR, EHFO)

The simple amplitude threshold does not characterize well the evoked events, hence we employed stricter discrimination. Two expert researchers revised the evoked potentials and selected events from every stimulation session, where the 40-500 Hz bandpass filtered evoked high frequency activity were similar to the ripple oscillations with at least 4 cycle described previously in the literature. We described these evoked activity as evoked ripples. Initially, we intended to evaluate the frequency of these selected ripple events. **Error! Reference source not found.**/A shows two example of the evoked ripples, and **Error! Reference source not found.**/B specify several other events excluded from the frequency analyzes.

Timing and duration

After the selection, we collected the peak latencies of the evoked ripples, as picking the highest peak on the Root Mean Squared, filtered (40-500 Hz) data after the stimulation 10-100 ms and the duration of the evoked ripple was calculated with time length while the RMS curve exceeded the half amplitude of this same height.

Frequency

The frequency components of the evoked events were measured with event-related spectral perturbation (ERSP from EEGLAB (Staba et al. 2007)) in a -150 ms to +150 ms window around the stimulation. The ERSP baseline was -150 to -50 ms before the stimulation, and the maximal frequency was 500 Hz. The highest peak of the time averaged ERSP is the middle of the evoked activity. The frequency with the maximal ERSP coefficients around the middle of the evoked event in a -25 ms, +25 ms time window is characterize the frequency components of the evoked activity. **Error! Reference source not found.**/C illustrates the method. On the averaged frequency curve, we identified the frequency peak with the largest power as primary frequency (signed with one white star on **Error! Reference source not found.**/C) and the lower peaks as the secondary frequencies for every events (signed with two and three white stars on **Error! Reference source not found.**/C). The primary and the secondary frequencies were sorted into bins from 20-650Hz counted by tens. On these frequency distributions gauss fitting were calculated using built in Matlab method in order to determine the mean and the standard deviation.

Phase-amplitude coupling of frequencies

Cross frequency coupling was calculated from all events of one stimulation session. The phase-amplitude coupling (PAC) was determined with calculating the modulation index (MI) (Tort et al. 2010) which quantifies the phase-amplitude coupling by measuring the distance of the phase-amplitude histogram of two given frequencies from the uniform distribution by means of Kullback-Leibler divergence. The original method applied Hilbert transformation on the filtered signal to get the phase information of one frequency and amplitude envelope of another filtered signal. Instead of this, the PAC values were calculated from the complex Morlet wavelet (phases and the corresponding amplitude values) of the 10-100 ms data after every stimulation from one session. The phase-amplitude histograms were calculated on every possible frequency

pairs from 11-968 Hz with 131 not evenly divided frequency bins and the phase were discretized into 18 bins, the mean of the corresponding amplitudes were calculated. The Kullback-Leibler divergence between the resulted mean histogram and the uniform distribution yield the MI value for every frequency pairs. The maximal MI value was determined from area (CA, DG, SUB) averages which designated one MI curve from the phase and one from the amplitude. These frequency-MI curves were considered as probability density functions, whereat mean and standard deviation were calculated. The frequencies which lied within the mean in one standard deviation were considered as significantly modulating (for phase) or modulated (for amplitude) frequencies. On the overall MI matrices paired t-tests (n=20, $p<0.001$) were applied for significant modulating-modulated frequency pairs. The Bonferroni-correction was not applicable, since the elements of the MI matrices are not independent. However, considering, that each MI matrix consists of 8515 values, for $p<0.001$ the expected number of false positive tests is 8.515, which should be randomly scattered in the matrix. Thus, the modulation was considered significant, if the number of positive tests far exceeded this expected number and showed patterned distribution in the MI matrix.

Multiple Unit Activity (MUA)

Multiple unit activity was calculated from the 20 kHz sampled data with band pass filtering (3rd order Butterworth) between 500 – 5000 Hz. After filtering and rectifying, Root Mean Square smoothing was computed with 11 ms window. The maximal value on this RMS curve after the stimulation artefact 10 ms to 100 ms was converted to statistical z-score (using the same method as in EHFA case, with the mean and standard deviation of the baseline). The laminar profile of the amplitude of the multiunit activity across channels was correlated to the amplitude of the evoked high frequency activity in all used recordings.

Methods – intracortical recording

Subjects

Subjects were recruited as part of an ongoing, multi-site collaborative project (Beth Israel Deaconess Medical Center, Brigham and Women's Hospital, Children's Hospital and Massachusetts General Hospital in Boston, and New York University Medical Center, New York, National Institute of Clinical Neurosciences). Eighteen patients with medically intractable epilepsy and frequent interictal discharges underwent subdural grid and/or depth electrode implantation for delineation of the seizure focus and eloquent cortex in preparation for removal of the epileptogenic region. The choice of patients for intracranial studies, the location of the clinical electrodes, duration of the implantation and, ultimately, the excision of cortex, were determined entirely on clinical grounds by an independent clinical team without regard for experimental considerations. Patients consented to the experimental procedure after a thorough explanation of the risks under procedures monitored and approved by the Institutional Review Boards at the respective centers in accordance with the Declaration of Helsinki. Determination of clinical etiology was made by the primary clinical team and, where possible, confirmed through pathological analysis of tissue removed at the time of resection.

The average age of the patients was 31.9 +/- 13 years. Etiologies spanned a wide range and included idiopathic causes, congenital cysts, artero-venous malformations, low grade tumors, cortical dysgenesis and mesial temporal sclerosis. Recordings were made from all cortical lobes: frontal (n=7), temporal (7, including neocortical and para-hippocampal), parietal (1) and occipital (3) cortex. Microelectrode arrays were placed according to surgical constraints. Based on determination of which subdural electrodes were within the seizure onset zone, microelectrodes were either in (n=7), near (within 2 cm) (n = 3) or far (n = 4) from the seizure onset zone.

Electrodes

For these investigations we utilized a novel system of microelectrodes to record activity in the human cortex. Details of electrode construction, recordings and analysis have been published previously (Ulbert et al. 2001). In brief, two types of laminar multielectrode arrays were employed here – depending on clinical situation. In most patients (n = 10) a short laminar probe was inserted into the gyral crown beneath or immediately adjacent to a subdural grid of electrodes. Schemes of positions are shown in Figure 4. Care was taken to insert the multielectrode perpendicular to the cortical surface in a location that previous non-invasive recordings indicated was highly likely to be within the seizure focus and, therefore, removed at the definitive surgery. The second type of electrode array was inserted through the center of a clinical depth electrode (Ad-Tech Medical Instrument Corporation, Racine, Wisconsin) and extended ~3.5 mm from the tip

of that electrode (n=4). This system was employed in patients receiving depth electrodes and was used to sample deep and medial structures. Both arrays comprised 24 contacts with diameters of 40 μm and intercontact distances of 150μm on centers.

Recordings

Differential recordings are made from each pair of successive contacts to establish a potential gradient across the cortical lamina. Details of the recording apparatus including amplifier and filter characteristics can be found in previous publications (Ulbert et al. 2001; Wang et al. 2005; Cash et al. 2009; Keller et al. 2010). In brief, after wideband (DC-10000Hz) preamplification (gain 10x, CMRR 90db, input impedance 10^{12} ohms), the signal is split into field potentials (filtered at 0.2-500Hz, gain 1000x, digitized at 2000Hz, 16bit) and multi-unit activity (MUA: filtered at 300-5000Hz, gain 1000x, digitized at 20000Hz, 12bit), and stored continuously with stimulus markers. These potential gradient recordings were used to estimate current source density (CSD) as discussed in Ulbert et al 2001. All steps of the analysis were performed using Neuroscan Edit 4.3 software (Compumedics, El Paso, TX) and with custom designed MATLAB (MathWorks, Natick, MA), LabVIEW (National Instruments Corp., Austin, TX) and C/C++ software as well as publicly available software suites (EEGLAB (Delorme and Makeig 2004)).

Selection of interictal discharges

Events were selected based on morphological characteristics typical in clinical practice for sharp waves, spikes, and spike-wave discharges (Niedermeyer 2005). Events with significantly higher amplitude than the baselineand showing biphasic or triphasic morphology with an initial fast phase of 200 ms or less followed by a prolonged, slower phase that lasted > 200 ms were chosen through manual inspection. Discharges were selected from epochs in which the patient was awake or drowsy. Although interictal spikes may be present in sleep we did not include such recordings in this analysis because they were not always available in each subject. Also eliminated from this analysis were events in or proximate to a seizure. Between 20 and 434 discharges were analyzed for each subject. Alltogether 1681 IIDs were involved in this analysis. This wide range of numbers was secondary to the high variability of discharge frequency between subjects, with an average rate of 13.8 and standard deviation of 11 discharges/min.

Selection of ripple oscillations

Detection of these oscillations was based on the method described by Crepon et al. and combined both automated and manual aspects (Crépon et al. 2010). After careful artifact rejection, putative ripple events were selected automatically by applying a 5 standard deviation (SD) threshold to the root-mean-square (RMS; 5ms sliding window) transformed bandpass filtered (zero-phase shift 4^{th} order Butterworth digital filter 80-500Hz) data (RMS data). To avoid the unnecessary detection of the same event recorded on multiple channels, co-occurring (less than 100ms) events were grouped on each multielectrode and the highest amplitude event in each group was selected for further analysis. These events were reviewed and either accepted or rejected by visual inspection. A custom designed graphical user interface (MATLAB) which allowed the reviewer (DF) to view the waveform and select based on waveform characteristics. In this way artifacts and spurious events were removed. The interface showed the filtered waveform, the scales from 80 to 500Hz of the morlet wavelet based continuous wavelet transformation of the unfiltered data, the filtered rectified waveform indicating significant peaks over 3 SD threshold and the RMS signal with indicated 5SD threshold line.

Using this method 427 ripples (ranging 17-98 per patient) was selected out of 8198 putative ripples (ranging 400-1608 per patient).

Because of the detection method each ripple event was associated with a single channel where it appeared with the highest amplitude. The distribution of this event over the channels was determined by statistical analysis. A channel was considered to have a ripple present when the RMS data exceeded 5SD threshold. Only a single channel had to have a visually determined ripple for an event to have been considered.

Time-Frequency analysis

Two types of time frequency analysis were used. Average time-frequency maps were calculated by modified event related spectral perturbation (ERSP) method provided by EEGLAB. Baseline activity was adjusted to the average spectral power over 1000ms EEG epochs containing no pathologic activities in between the analyzed events. Spectral power was displayed in decibel values.

Single epoch time-frequency activity for both ripple central frequency measurement and continuous time frequency decomposition was performed by continuous morlet wavelet transformation ("Wavelet software was provided by C. Torrence and G. Compo; URL: http://atoc.colorado.edu/research/wavelets/"). The wavelet coefficients were averaged in time within a 100ms window surrounding the HFA event and the frequency value with highest wavelet coefficient in the 80-500 Hz range was selected as central frequency of the ripple or HFA.

Timing of different HFA or IID components

To determine the timing of the HFA, or IID we used the absolute recording times of either the peak and the steepest slope of the HFA envelope or the IID. The HFA envelope was found by calculating the RMS of the band-pass (80-500 Hz) filtered signal. The steepest slope was determined by selecting the local maxima of the first derivative of HFA envelope in time. Later we calculated differences of these time values. The reference point was the time of the ripple envelope peak on the third laminar channel (channels are numbered from the pia surface).

Standardizing the electrode penetration

Because of clinical considerations, we did not have complete histological reconstruction of the track left by electrode array in the tissue. We therefore relied on our previous findings (20), and used the electrophysiological characteristics of the data to decide how deep the penetration was. Cortical surface was determined by a sudden drop of IID amplitude and an apparent appearance of slow artifacts indicating that the electrodes above a certain level were surrounded by CSF.

Current source density and multiple unit analysis

Current source density (CSD) was calculated from 2kHz sampled local field potential data (LFP). Before applying spatial derivation a hamming window based spatial filter was applied to compensatefor artificial spatial inhomogenities. Multiple unit activity (MUA) was calculated as the high frequency (500-5000Hz) power activity from 20kHz sampled data using digital filter and rectification.

Methods HFO and memory performance in TLE patients.

10 TLE patients undergoing presurgical evaluation with foramen ovale electrodes were enrolled in the study (n=10; left HS:7, right HS:3). Three versions of the Rey Verbal memory task was administered on three nights to the participants. The objective of this task is to learn a list of 15 words within 5 consecutive learning rounds. Delayed memory recall was measured 30 minutes after the last (5th) learning round; morning memory recall was measured after waking in the next morning. Sleep stages were detected, sleep efficiency was measured. Fast and slow sleep spindles were detected with automated threshold-cutting method based on individually adjusted spindle frequency values.

Variation of individual memory performance and group averages were correlated to the number of sleep spindles in nREM sleep. Linear regression between memory retention and the number of sleep spindles was also calculated.

Results – intrahippocampal evoked potentials

Evoked potentials in the hippocampus

Figure 1 demonstrates an example of evoked potential in the hippocampus in P33. A series of events was observed in the subiculum at 5ms, that around the fissure hippocampi at 20ms, that corresponded the synaptic activation time of perforant path.

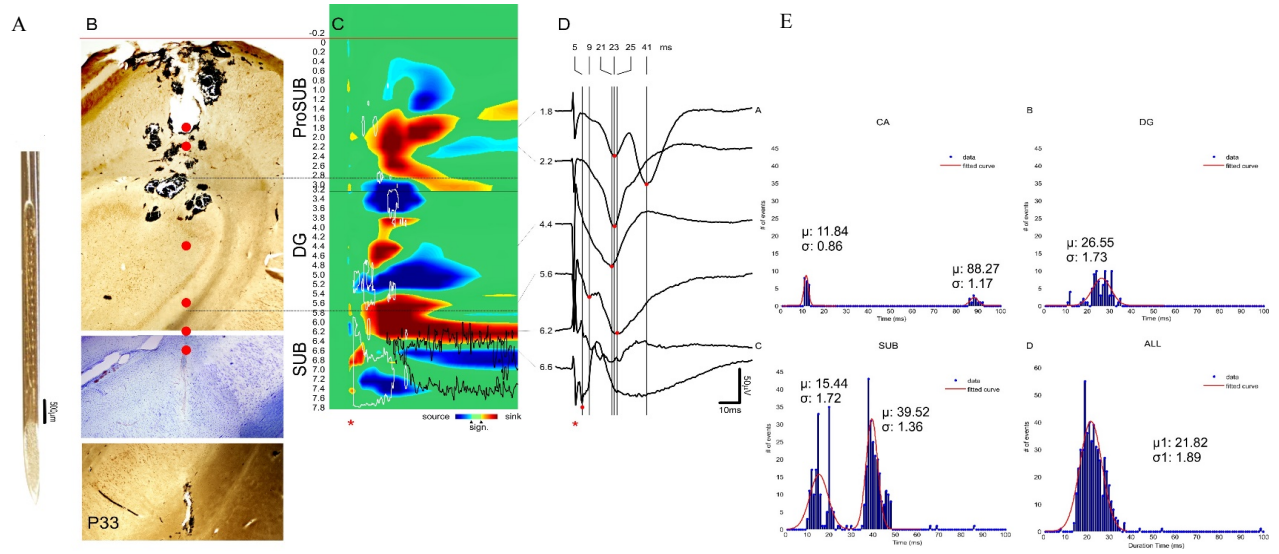

Figure 1 Visualization of the recording situation. A) A picture of the microelectrode. B) Photo of the hippocampal slice from P33, where the red line sign the surface of the hippocampus, and the red dots show the electrode penetration track and P33 histological reconstruction is shown. The electrode trajectory in the tissue. GluR2-3 immunhistochemistry, and Nissle staining. C) CSD, and MUA map of evoked potential (15mA stim.). Red: sink, blue: source, white contour: MUA increase, black contour: MUA decrease. D) The order of the sinks in different depth indicating the peak latencies. E) Latencies of evoked HFO oscillations in the different subregions of the hippocampus. The most frequent latency was around 10-30 ms. Dashed line: border between regions. Red line: ependymal surface, Asterix: stimulus, CSD: current source density, MUA multiple unit activity, SUB: subiculum, DG: dentate gyrus, ProSub: prosubiculum. Sub I: proximal part of the Subiculum, Sub II: distal part of the subiculum.

Evoked short latency ripples in the hippocampus

We applied short electrical stimuli to evoke potentials and fast oscillation in the human hippocampus during temporal lobectomy surgery of therapy resistant epilepsy patients under general anaesthesia. Investigation arrangement is depicted on Figure 2 A/B. Briefly, one or two laminar probes were introduced into the intact hippocampus while clinical ECoG strip was places around the temporal pole to the temporo-basal area. Low frequency electrical pulses (0.5 Hz, 5-10-15 mA, 0.2 ms pulse duration, 25 or 50 stimuli) were delivered to the adjacent contacts of the ECoG electrode.

Evoked fast activity appeared over the cortico-hippocampal evoked potential (CHEP) within 100ms latency (Figure 2/B). Figure 1/E shows the latencies in different regions of the hippocampus. The majoritiy of the evoked HFO oscillations occurred whithin 30ms. Some longer latencies were observed in the subiculum, that could have been the result of a more lateral position of the strip electrode. Figure 2/C shows the filtration and statistical methods to detect high frequency activity in the 80-500Hz range (HFA). Evoked 80-500Hz HFA showed layer specific distribution within the hippocampus (Figure 2/D). The precise histological reconstruction of the electrode trajectory made us possible to compare the layer selectivity with the histological layers of the hippocampus. One example (P22) is shown on figure 2. Evoked high frequency activity in this case was localized to app. 1 mm (3200-4200μm) that correlated with the dendritic layer of the subiculum. The dendritic localization was strengthened by calculation of multiple unit activity. MUA reflects the 500-3000Hz frequency range in the field potentials that is generated by asynchronous firing of the surrounding units. In P22 the MUA located beneath the HFA area partially overlapping with it but matching perfectly the anatomical cell layer (Figure 2/E). On the contrary we can conclude that the vast majority of the 80-500Hz HFA activity is different from the MUA. This does not mean that MUA activity, which is a wide range high frequency activity arising from asynchronously firing neurons, missed the 80-500Hz range selectively. We used a 5SD threshold as a measure of significant HFA. All the cell layers, especially in the subiculum performed significant HFA (Figure 3, Figure 2/E), but the pure HFA layers sometimes missed MUA range activity (e.g. Figure 2/E 1800-2200μm).

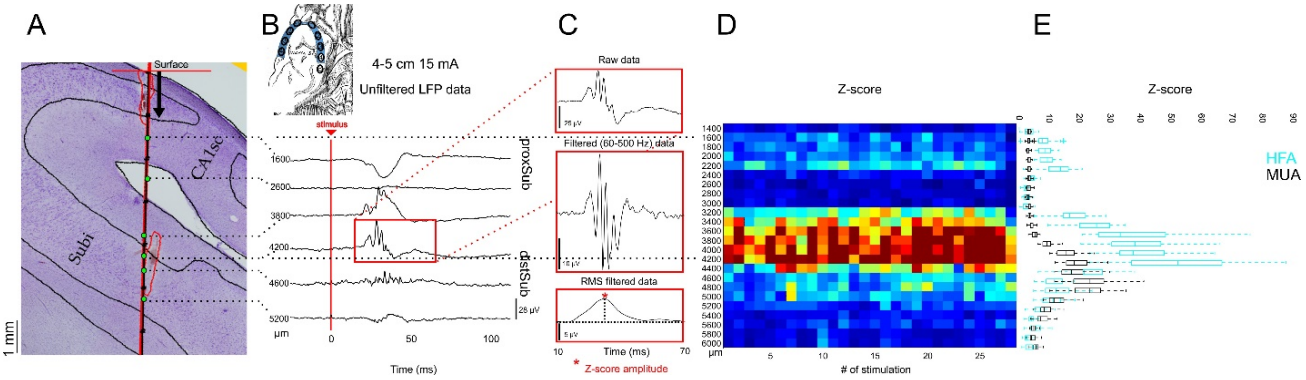

Figure 2. Note that parts A, D and E are arranged to match the depths (dotted line across part B and C at 1600 and 4200µm). 15 Sample of a Hippocampus slice and recorded evoked potential from Pt22. A) Histology indicates Subiculum (Subi) and CA1sc subregions. B) Local field potential gradients originate from the green electrode contacts. Data in the red box analyzed in the magnified red boxes in C. The red vertical line indicates the time point of the stimulation. C) Illustration of the evoked potential analysis. The raw event is on the top, the bandpass filtered form is in the middle and the RMS of it is on the bottom, where the red dot shows the maximal value, which we take as the middle of the evoked activity. This maximal values are converted into z-scores and plotted on D. D) The z-score of the EHFA after every stimulation is color coded and plotted. E) Laminar profile of the z-score value distribution of EHFA (blue) and MUA (black).

Figure 3 and Table 1 summarizes the eight patients involved in the analysis. Out of fourteen patients recorded three cases were rejected due to missing or low quality histological reconstruction, two cases were excluded because the stimulation protocol was compromised (applied after partial resection of the temporal lobe), and one case was left out due to noisy recording. HFA was present in all types of sampled hippocampal subregions.

Patient code	Age (y)	Side	Gender	Duration of epilepsy (y)	MRI finding	Hc damage	Electrode localization	Anesthesia	Outcome	Follow up (y)
P17	31	Right	m	22	Right HS	sHS	body	Isoflurane	1B	3
P22	46	Left	f	10	Bilateral HS	sHS	digitations	Propofol	3A	9
P25	36	Left	f	6	Left HS	sHS	head	Propofol	1A	3
P26	40	Right	f	26	Bilateral HS	sHS	body	Isoflurane	2B	3
P33	51	Left	f	32	TU (left amygdala)	mHS	head	Propofol	3A	2
P36	39	Left	f	38	Left HS	sHS	body	Propofol	1A	9
P38	57	Left	m	23	Left HS	mHS	body	Isoflurane	1A	5
P47	38	Left	f	3	Left FCD + HS	mHS	head	Propofol	1A	6

Table 1. Summary of eight patients involved in analysis of evHFO.

Table 2 summarizes the regions of the sampled hippocampi. We defined a special area in the hilus region in cases where the electrode travelled in the vicinity of the granule cell layer of the DG without crossing it (beyond the limb of one blade of DG). In these points we were unable to discriminate between hilar, DG and CA3c participation.

Figure 2 shows the successful recordings (all of them) where we were able to analyze the evoked responses. We observed that all the recordings contained significant HFA and all the mentioned areas (CA, DG, Sub) were active in it. The most sampled region was the subiculum (n=6), and in all cases it was active and very often contributed to the highest percentages in the hippocampus.

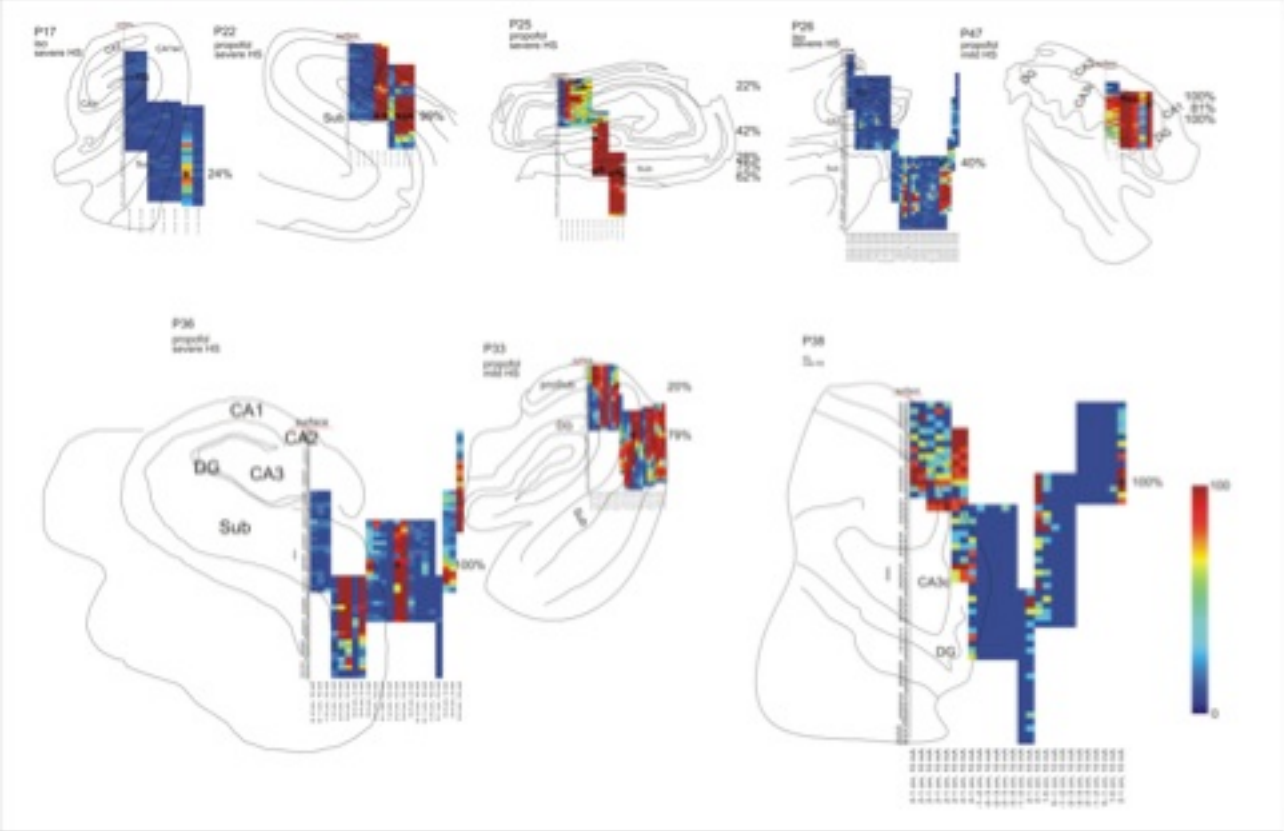

Figure 3. Depth dependency of the evoking probability of HFA within the hippocampus in all the sampled cases. Vertical bars show the sampled portion of the hippocampus, underneath the stimulation parameters. All vertical positions must be projected to the electrode trajectory in the middle. Black asterisks show the depths of visual ripple detection. Percentage values on the right indicate the probability to evoke a ripple within the HFA activity. Color bar can be found on the left. Note that subiculum was always activated, mostly with the highest percentage values.

CA2	P17, P25, P26, P47, P38
CA3	P26, P36,
CA3c	P17, P25, P47, P38
DG	P17, P25, P33, P47, P38
Hilus/DG/CA3c special hilar	P25, P26, P47, P38
Sub	P17, P22, P25, P26, P36, P33

Table 2. Hipocampal subregions sampled in different experiments.

Variability of the HFA activity

Significant HFA was not uniform. As we mentioned, pure MUA was enough to be detected as HFA. But HFA activity detected outside the neuronal layers showed significant variance also. Figure 3 shows the spots in the hippocampal map of HFA where visually detected ripples were identified. Number values indicate that in these cases the ripple activity was evoked with high fidelity.

Figure 4 shows some examples to the various types of detected HFA activity outside the MUA layers. Part A and C show evoked potentials containing ripple oscillation based on our visual selection method. Part C contain examples for (a) no HFA activity, (b) evoked HFA in the ripple range that is too short for being classified as ripple, (c) high amplitude sharp transient, (d) slow -, and (e) burst-firing unit (interneuron). Detection of ripple oscillation was indicated with astrisks on Figure 3.

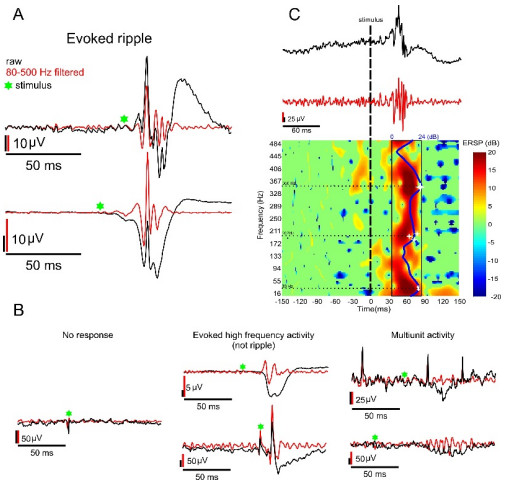

Figure 4. Selection of evoked high frequency oscillation and illustration of the method for analysis of the frequency components. A) Visually selected evoked potentials identified as ripple, black line signs the raw data, red line signs the 80-500 Hz filtered data and green star signs the time of the stimulation. B) Examples of excluded events, like no response, evoked high frequency activity and multiple unit activity. C) Illustration of the ERSP of the event on the top (black line). The blue line stands for the maximal amplitude frequency component curve, whereas the white starts and the dotted lines sign the maximal values (360 Hz, 39 Hz, 207 Hz).

Input-output relationship of evoked ripples

Figure 5 illustrates the stimulation site and strength dependency of the evoked ripples in the various subregions of the hippocampus. To determine the stimulation site we used a semi-quantitative method. Since the exact location of the strip was not visualized, we identified the anterior-most point of the strip bending around the temporal pole. All the points beyond this one were recalculated according to the distance from this point. So the anterior-posterior distance from the temporal pole was estimated with reasonable (centimeter) precision. The medial-lateral position of the strip was not controlled, so, especially the more posterior positions, may have higher variability in this extension. Having this uncertainty in mind, we may say that the most effective stimulation point was between 1-5cm beyond the pole.

Evoking probability was less sensitive to the changes of the stimulation strength.

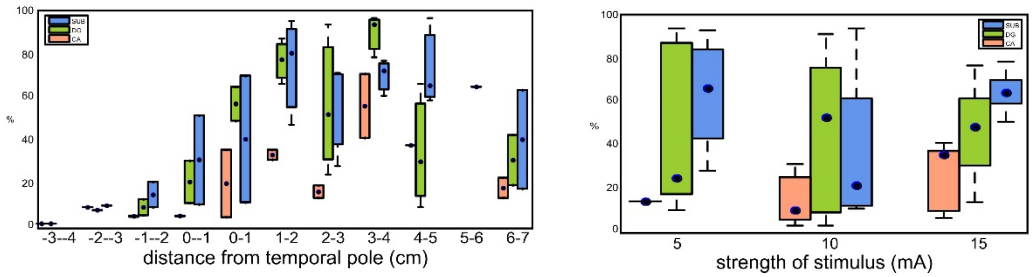

Figure 5 Stimulus site and strength dependency of EHFA activity in the hippocampus. Note the clear site selectivity. Stimulus strength was not that affective.

Analysis of the frequency distribution

To analyze the frequency components of the CHEPs, we used event related spectral perturbation (ERSP from EEGLAB (Delorme and Makeig 2004)). Highest power frequency peaks were measured on time-averaged (in a 50ms window around the maximal peak of the event) ERSP values.

We classified the maximal power amplitude frequency values as first frequency values and the lower ones as secondary frequency peaks of every events and sorted into frequency bins from 20 to 650 Hz. Figure 6 shows the results. In the CA region (Figure 6/A), the main distribution of primary frequencies was in the slow ripple range (95.75±10.46Hz; range: 66-130Hz) and a relatively separated subset was in the gamma range (27.53±12.75Hz; range: 20-46 Hz). The secondary frequencies were in the fast ripple range (200±4.98Hz; range: 170-493 Hz). The frequencies of DG showed (Figure 6/C) slightly different distribution shifted more to the fast ripple range. The most prominent first frequencies were around 15 ±50 Hz, 108.3±10.8 Hz and 194.4 ±10.34 Hz. The secondary frequencies reflected the same trend, the highest incidence was around 206.7±4.1 Hz and 303.7 ±6.1 Hz. Most of the events occurred in the Subiculum (n=386), and the primary frequencies of these showed bimodal distribution (Figure 6/B) with peak around

45±11.52 Hz and 166.9±48.01 Hz. The secondary frequencies had similar distribution, highest peak around 41.8 ±8.9 Hz and 169.8±21.76 Hz which draw a long tailed distribution with almost 500 Hz maximal value. In summary (Figure 6/D) we found a bimodal distribution in the primary and secondary frequencies. The primary frequencies were most prominent around 41.5 ±14.1 Hz and 172.8±48.8 Hz while the secondary had 40.3±10.8 Hz and 186.4 ±30.5 Hz with a long tailed distribution which reached 500 Hz.

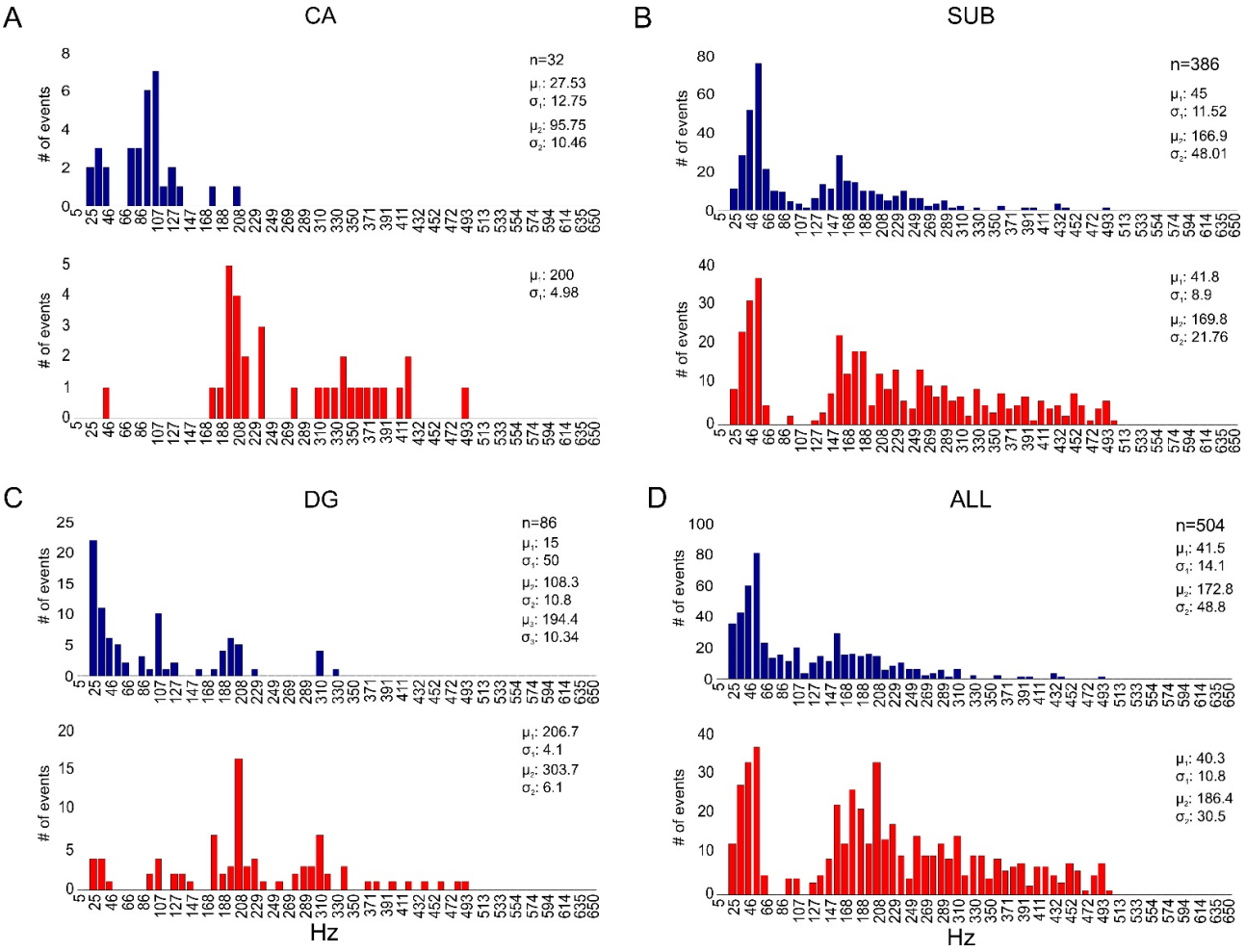

Figure 6 Frequency distribution of ripple events in the hippocampal regions. The highest proportion of fast ripples appeared in the subiculum. Secondary peaks of the spectrum was determined in order to analyse combined frequencies. 30-50Hz gamma activity was consequently detected in all regions.

Cross Frequency Coupling

We analyzed the interaction of the frequencies. Figure 7 illustrates the mean modulation index (MI) as a measure of phase-amplitude coupling between the frequencies from 11 to 968 Hz grouped by the regions. The three regions show slightly different coupling patterns. In CA, the most influential frequencies were between 11-33.4Hz (peak around 20Hz), affecting frequencies in the range of 14.6-322.7Hz (n=2). In DG similar interaction is between 11-57.3Hz (as modulating) and 47-478.9Hz (peak around 400Hz as modulated) frequencies. The Sub is very similar to DG, with 11-35.9Hz influencing and 46.3-507.7Hz modulated frequency range (peak around 230Hz). The volume of this effect is the highest in the DG (max MI values: 0.4), followed by the Sub (max MI: 0.25), and the lowest is in the CA (max MI: 0.14). The background activity reveals poor MI values in all areas with an interesting, but very small coupling between gamma band (15-80 Hz) and the multiple unit activity range (684-968 Hz).

Statistical analysis resulted significant difference between active and background activity in terms of interaction of 11-60Hz range modulating the 30-814Hz range during the active phase. Interestingly significantly increased modulation was measured as [85-160 Hz and 575-968 Hz] ranges modulated the [814-968Hz] range during resting condition (Figure 7 bottom right grey stripped areas).

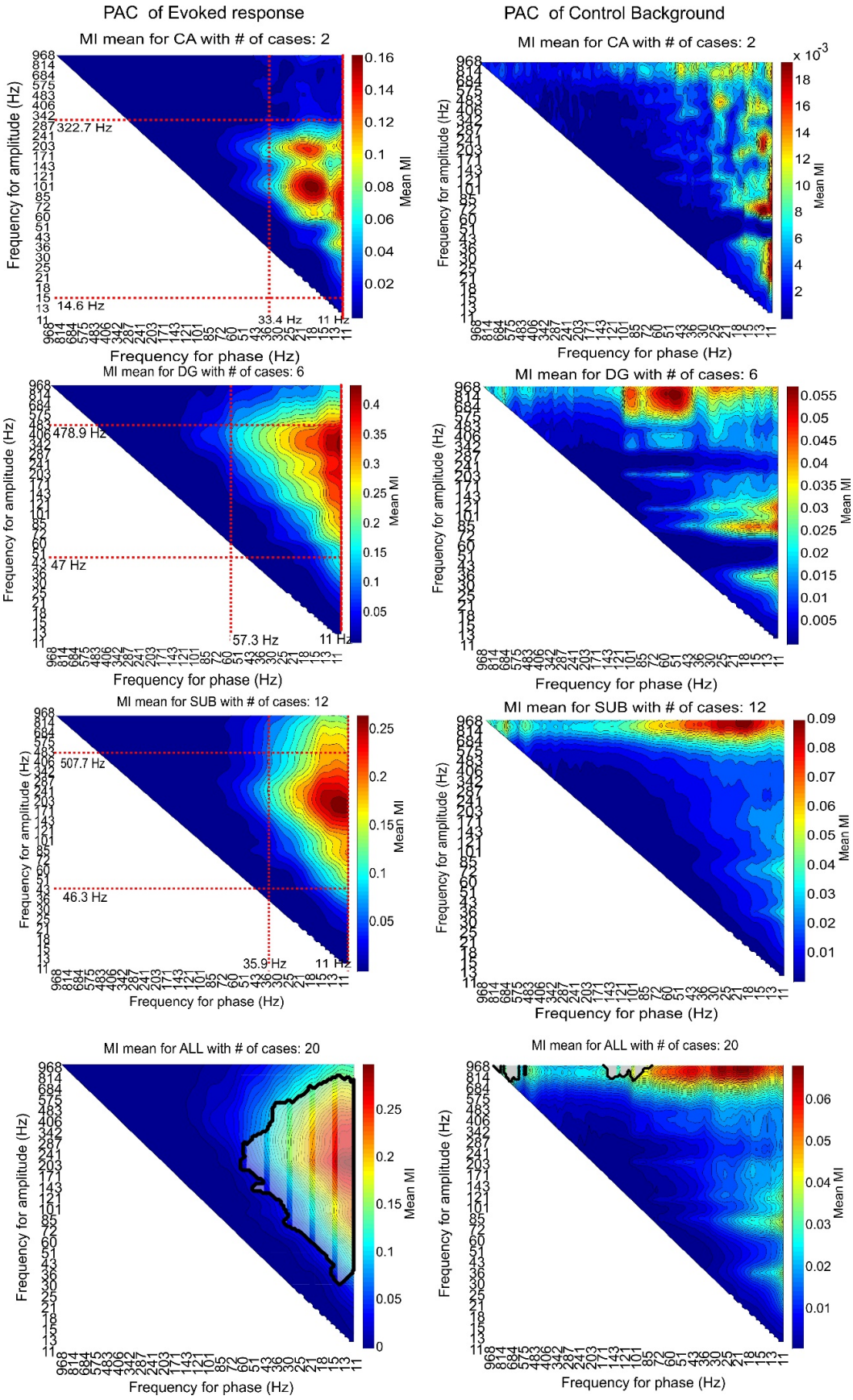

Figure 7 Cross frequency coupling during evoked ripples and their background activity averaged by hippocampal regions CA, DG, SUB and all. The modulation index (MI) values sign the strength of the phase-amplitude coupling, the hotter color represents stronger relation between the phase of the frequency on the horizontal axis, and the amplitude of the frequency on the vertical axis. The red dotted lines and the black line framed, striped area represents the limits of the most significantly influential and affected frequencies. The left column contains the results of the evoked ripples, while the right column shows the frequency coupling of the background activity.

Results 2 - Intracortical distribution of interictal discharge related HFO

The relationship between the IID and the high frequency activity is variable.

We performed continuous time frequency analysis of IIDs to study the variability of the HFA power within a single case. Figure 8/A shows the band pass filtered (0.5-30Hz) IID activity (bellow) and the time frequency map (80-500Hz, above) of consecutive IIDs in a representative case. Note the differences of high frequency activity (HFA) from discharge to discharge. There were IIDs that had no or very modest HFA (first IID on Figure 8/A) and ones with high power of HFA (2^{nd}-4^{th} IID on the figure 8/A). Only the 4^{th} IID on the figure had HFA regular enough to be detected as a ripple by the visual detection method (enlarged on Figure 8/B).

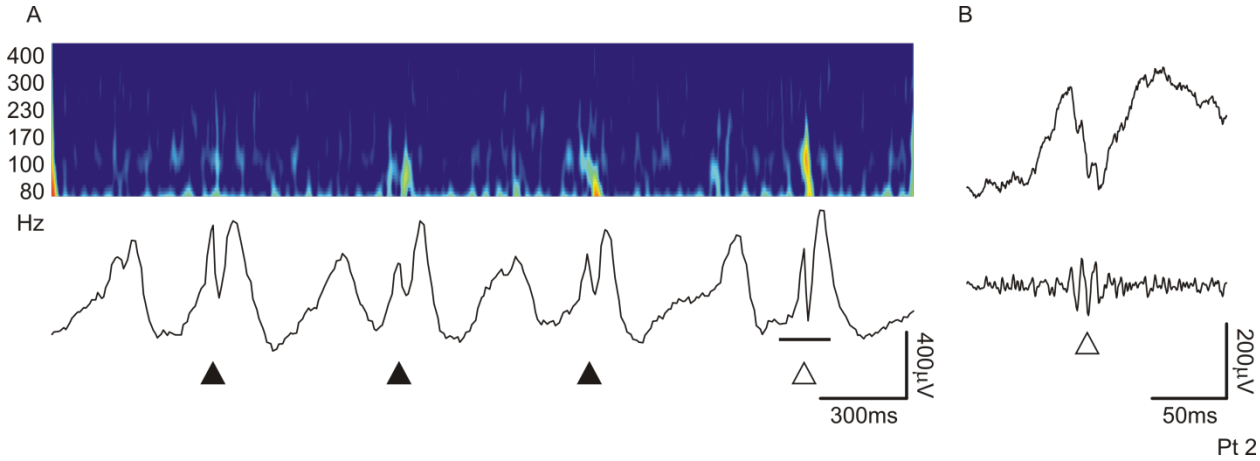

Figure 8. – Continous ongoing activity with IIDs and ripple. A) Bottom: Example of ongoing slow activity with IIDs (triangles). Band-pass filtered (0.5-30Hz) field potential gradient recording from layer II-III of the neocortex. Above: continuous wavelet transformation of the original signal in the 80-500Hz range. Note the difference in the 100-130 Hz range between IIDs. The difference is not simply a function of the amplitude of the sharp component of the discharge, and the maxima are located to the transition period between the IID's positive and negative deflection. (Positive upwards.) Note that only the IID marked by open triangle contained a high frequency event that have been called ripple based on the visual detection. B) Above: Unfiltered portion of the trace indicated by the black segment and the open triangle. Bottom: Bandpass filtered (80-500Hz) waveform.

Ripples are detected with laminar microelectrode arrays

Discernable ripple oscillations were observed in 8 subjects using the visual oscillation counting approach. We reviewed 8439 putative oscillations in 113.9 min of recording. 427 ripple oscillations were selected. The across subject average ripple rate was 3.8/min (which varied between 0.6/min and 11.9/min per patient).

Fast ripples in the neocortex and in the mesial temporal lobe were different in rate and appearance

The proportion of the fast ripples compared to the slow ripples was greater in hippocampus than in the neocortex (Figure 10/A). Some examples of such fast ripple activity are shown in Figure 10 in order to make a comparison between these two types of recordings. The neocortical fast ripples had smaller amplitude, less rhythmicity, and, based on the unfiltered traces, seem to also include nonrhythmic unitary events. It is also important to note that the displayed neocortical fast ripple is one of the best examples from all such recordings, whereas high quality fast ripples were comparatively common within the mesial temporal lobe of multiple subjects.

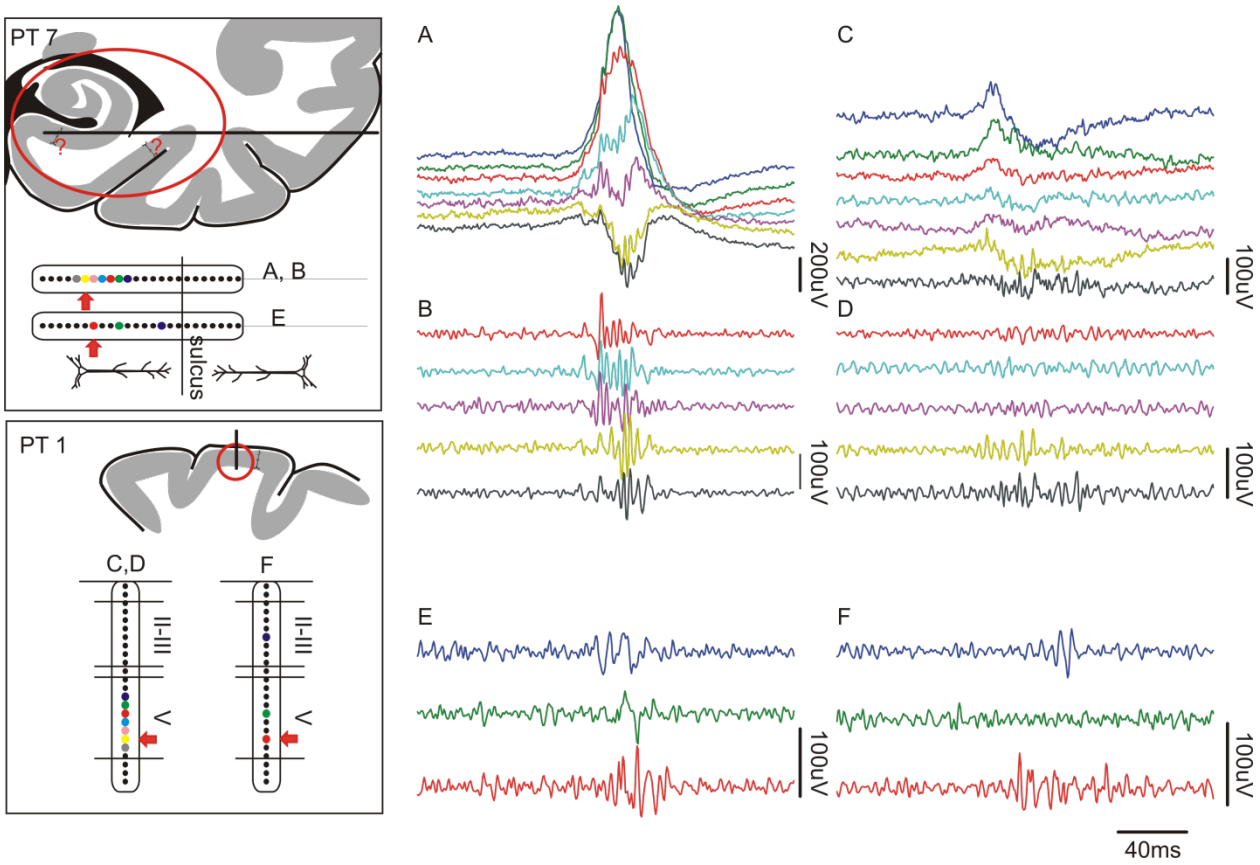

Figure 10 - Examples of fast ripples in the temporo-mesial and neocortical structures. Left column: Schematic diagram of recording sites. Top panel: Estimated location of deep laminar multielectrode in the temporo-mesial structures. Bottom panel: Thumbtack multielectrode in the occipital lobe. Insets indicate the approximate location of the recording contacts compared to electro-physiologically identified landmarks. (see method for details). Colored contacts correspond to the colored line on right hand site of the figure according to the letter of the actual panel indicated near the inset. Fast ripples were detected on channel indicated by a red arrow. (See methods for details.) A) and C) Examples of fast ripple associated IID in the temporo-mesial and neocortical recording sites respectively. (Filter high pass 2Hz) B) and D) same IIDs as in A) and C) with band pass filter 80-500Hz, Note that the neocortical fast ripple is lower in amplitude has fewer channels involved and - especially on the wide band filtration - more irregular, less like a sinusoid oscillation and more like harboring some solitary neuronal events too beside the field potential oscillation. E) and F) IIDs with fast ripple in the depth and slow ripple on the more superficial electrodes in the temporo-mesial and neocortical recording sites respectively. Note that the deep fast ripple precedes the surface slow ripple in the neocortex, while the timing is just opposite in the mesial temporal lobe.

Coalescence of different ripple frequencies, and their distribution over neocortical domains

The cortical involvement was determined by applying 5 SD rule over every intracortical channels for each ripple oscillation. Beside the highest power (primary or central) frequency we calculated the secondary peaks also, and compared the distributions (Figure 11). We analysed the IID dependent and IID independent ripple events separetelly. We observed that the IID dependent event contain a well defined ripple component in the upper layers between 80-130Hz range. The fast ripple components of the IID depenent ripples located also the upper cortical layers. The IID non dependent ripples lacked the above mentioned slow ripple component and both the primara both the secondary peaks spanned to the fast ripple range and located relatively deeper.

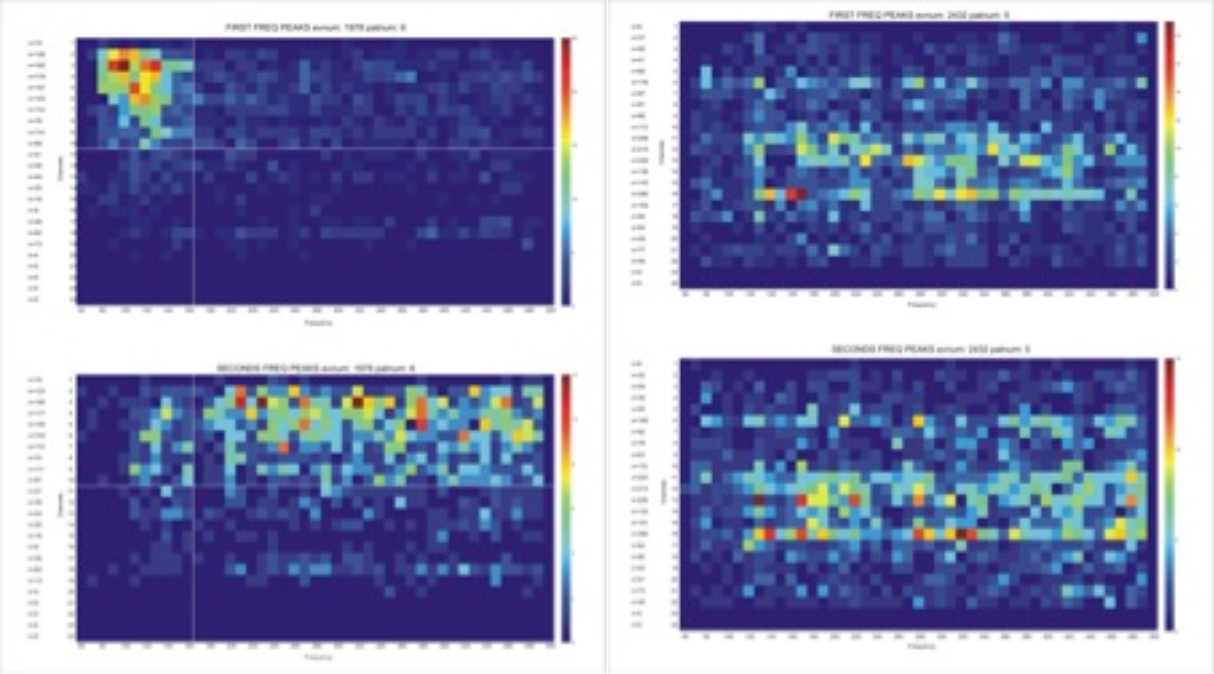

Figure 11 Transcortical frequency distribution of ripple oscillations. Left panels show IID dependent, right panels show IID independent ripples. Upper panels refer to primary frequencies, lower panes the secondary frequencies.

Results 3 - Relationship of HFO and memory performance of TLE patients.

The rate of forgetting was measured by extracting performance in the learning session from the performance in the morning recall. Correlation between the rate of forgetting and the number of sleep spindles during overnight sleep showed significant positive correlations with the number of spindles on electrodes: C3, C4, P3, P4, O1, and O2. Retention between the last learning round and morning recall showed significant negative correlations with the number of sleep spindles on electrodes P3, P4, O1, O2.

When only participants with retention 0 or higher were taken into the analysis, retention between the delayed memory recall and morning recall showed a great number of significant negative correlations with the amount of sleep spindles, mostly on frontal and central electrode sites. Also, variance analysis showed that when retention was 0 or higher, spindle number on F4 (F=10.54; p=0.08), C3 (F=8.83; p=0.002), C4 (F=376.62; p=0.03), P3 (F=54.91; p=0.09) and P4 (281.59; p=0.04) electrode sites showed a significant modulatory effect on the amount of retention. However, a very small number of participants showed increase in memory retention (retention: delayed-morning n=3; last learning round morning n=1), moreover most participants performed worse on the morning recall, compared to their performance on the previous night.

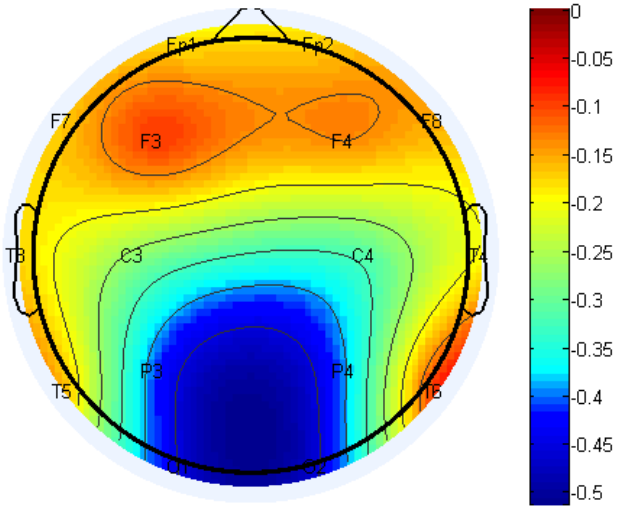

Figure 12. Retention between the last learning round and morning recall showed significant negative correlations with the number of spindles on electrodes P3, P4, O1, O2.

Conclusions

We investigated human epileptic patients with implanted macro-, and microelectrodes to study high frequency oscillation (HFO). Our main result is that we were able to describe short latency evoked HFO (sleHFO) in the hippocampus (Hc) as a response to cortical electric stimulation. All the hippocampal areas were able to perform sleHFO, but subiculum was the most active and highest in frequency. The subicular activation seemed to depend on the severity of hippocampal sclerosis with cell loss in the CA1 area. Using similar microelectrodes in awake conditions we described the HFOs associated to epileptic spikes (ES) in the neocortex. We described a subgroup of HFO that follows ESs selectively in the upper cortical layers around 100-130Hz. We tried to link hippocampal, or cortical MFOs to memory performances but we found that the sleep spindle -, and thus hypothetically MFO-, dependent memory processes change in epilepsy that we require more research in patients to study sleep spindles without invasive electrodes to conclude our results.

As a conclusion we gained higher understanding on the cortical and hippocampal organization of epilepsy specific HFOs, that helps to understand the generation of epileptic seizures. Based on these results we might be able to utilize a new stimulation paradigm to study the epileptogenic nature of the hippocampus in epileptic or general neurosurgical cases.

References

Amzica F, Steriade M. Short- and long-range neuronal synchronization of the slow (. Journal of Neurophysiology. 1995 Jan;73(1):20–38.

Bragin A, Engel J, Wilson CL, Fried I, Buzsáki G. High-frequency oscillations in human brain. Hippocampus. 1999;9(2):137–42.

Bragin A, Wilson CL, Almajano J, Mody I, Engel J. High-frequency oscillations after status epilepticus: epileptogenesis and seizure genesis. Epilepsia. 2004 Sep;45(9):1017–23.

Buzsáki G, Horváth Z, Urioste R, Hetke J, Wise K. High-frequency network oscillation in the hippocampus. Science. 1992 May 15;256(5059):1025–7.

Cash SS, Halgren E, Dehghani N, Rossetti AO, Thesen T, Wang C, et al. The human K-complex represents an isolated cortical down-state. Science. 2009 May 22;324(5930):1084–7.

Clemens Z, Fabó D, Halász P. Overnight verbal memory retention correlates with the number of sleep spindles. Neuroscience. 2005;132(2):529–35.

Clemens Z, Fabó D, Halász P. Twenty-four hours retention of visuospatial memory correlates with the number of parietal sleep spindles. Neurosci Lett. 2006 Jul;403(1-2):52–6.

Clemens Z, Mölle M, Eross L, Barsi P, Halász P, Born J. Temporal coupling of parahippocampal ripples, sleep spindles and slow oscillations in humans. Brain. 2007 Nov;130(Pt 11):2868–78.

Clemens Z, Mölle M, Eross L, Jakus R, Rásonyi G, Halász P, et al. Fine-tuned coupling between human parahippocampal ripples and sleep spindles. Eur J Neurosci. 2011 Feb;33(3):511–20.

Crépon B, Navarro V, Hasboun D, Clemenceau S, Martinerie J, Baulac M, et al. Mapping interictal oscillations greater than 200 Hz recorded with intracranial macroelectrodes in human epilepsy. Brain. 2010 Jan;133(Pt 1):33–45.

Csercsa R, Dombovári B, Fabó D, Wittner L, Eross L, Entz L, et al. Laminar analysis of slow wave activity in humans. Brain. 2010 Sep 1;133(9):2814–29.

Delorme A, Makeig S. EEGLAB: an open source toolbox for analysis of single-trial EEG dynamics including independent component analysis. J Neurosci Methods. 2004 Mar 15;134(1):9–21.

Engel J, Bragin A, Staba R, Mody I. High-frequency oscillations: what is normal and what is not? Epilepsia. 2009 Apr 1;50(4):598–604.

Fabó D, Maglóczky Z, Wittner L, Pék A, Eross L, Czirják S, et al. Properties of in vivo interictal spike generation in the human subiculum. Brain. 2008 Feb 1;131(Pt 2):485–99.

Heit G, ULBERT I, Halgren E, Karmos G, Shuer L. Current source density analysis of synaptic generators of human interictal spike. Stereotact Funct Neurosurg. 1999;73(1-4):116.

Jacobs J, Levan P, Chander R, Hall J, Dubeau F, Gotman J. Interictal high-frequency oscillations (80-500 Hz) are an indicator of seizure onset areas independent of spikes in the human epileptic brain. Epilepsia. 2008 Nov 1;49(11):1893–907.

Jacobs J, Zelmann R, Jirsch J, Chander R, Dubeau C-ÉCF, Gotman J. High frequency oscillations (80-500 Hz) in the preictal period in patients with focal seizures. Epilepsia. 2009 Jul;50(7):1780–92.

Jacobs J, Zijlmans M, Zelmann R, Chatillon C-E, Hall J, Olivier A, et al. High-frequency electroencephalographic oscillations correlate with outcome of epilepsy surgery. Ann Neurol. 2010

Feb;67(2):209–20.

Keller C, Truccolo W, Gale J, Eskandar E, Thesen T, Carlson C, et al. Heterogeneous neuronal firing patterns during interictal epileptiform discharges in the human cortex. Brain. 2010 Jun 1;133(6):1668.

Niedermeyer E. Abnormal EEG Patterns: Epileptic and Paroxysmal. In: Niedermeyer E, Lopes da Silva FH, editors. Electroencephalography: basic principles, clinical applications, and related fields. Fifth. Philadelphia: Lippincott Williams and Wilkins; 2005. pp. 255–81.

Ramadan W, Eschenko O, Sara SJ. Hippocampal sharp wave/ripples during sleep for consolidation of associative memory. PLoS ONE. 2009;4(8):e6697.

Sirota A, Csicsvari J, Buhl D, Buzsáki G. Communication between neocortex and hippocampus during sleep in rodents. Proc Natl Acad Sci USA. 2003 Feb 18;100(4):2065–9.

Staba RJ, Frighetto L, Behnke EJ, Mathern GW, Fields T, Bragin A, et al. Increased fast ripple to ripple ratios correlate with reduced hippocampal volumes and neuron loss in temporal lobe epilepsy patients. Epilepsia. 2007 Nov 1;48(11):2130–8.

Staba RJ, Wilson CL, Bragin A, Fried I, Engel J. Quantitative analysis of high-frequency oscillations (80-500 Hz) recorded in human epileptic hippocampus and entorhinal cortex. Journal of Neurophysiology. 2002 Oct 1;88(4):1743–52.

Staba RJ, Wilson CL, Bragin A, Jhung D, Fried I, Engel J. High-frequency oscillations recorded in human medial temporal lobe during sleep. Ann Neurol. 2004 Jul 1;56(1):108–15.

Tort ABL, Komorowski R, Eichenbaum H, Kopell N. Measuring phase-amplitude coupling between neuronal oscillations of different frequencies. Journal of Neurophysiology. 2010 Aug;104(2):1195–210.

Ulbert I, Karmos G, Heit G, Halgren E. Early discrimination of coherent versus incoherent motion by multiunit and synaptic activity in human putative MT+. Human brain mapping [Internet]. 2001;13(4):226–38. Available from: http://eutils.ncbi.nlm.nih.gov/entrez/eutils/elink.fcgi?dbfrom=pubmed&id=11410951&retmode=ref&cmd=prlinks

Ulbert I, Maglóczky Z, Eross L, Czirják S, Vajda J, Bognár L, et al. In vivo laminar electrophysiology co-registered with histology in the hippocampus of patients with temporal lobe epilepsy. Exp Neurol [Internet]. 2004 Jan 8;187(2):310–8. Available from: http://eutils.ncbi.nlm.nih.gov/entrez/eutils/elink.fcgi?dbfrom=pubmed&id=15144857&retmode=ref&cmd=prlinks

Urrestarazu E, Chander R, Dubeau F, Gotman J. Interictal high-frequency oscillations (100-500 Hz) in the intracerebral EEG of epileptic patients. Brain. 2007 Sep 1;130(Pt 9):2354–66.

Valentín A, Alarcon G, Garcia Seoane JJ, Lacruz ME, Nayak SD, Honavar M, et al. Single-pulse electrical stimulation identifies epileptogenic frontal cortex in the human brain. Neurology. 2005 Aug 9;65(3):426–35.

Wang C, Ulbert I, Schomer DL, Marinkovic K, Halgren E. Responses of human anterior cingulate cortex microdomains to error detection, conflict monitoring, stimulus-response mapping, familiarity, and orienting. Journal of Neuroscience. 2005 Jan 19;25(3):604–13.